# Evaluation of the Laser-Induced Thermotherapy (LITT) treatment effect of breast cancer based on tissue viscoelastic properties

Jiayao Chen[1#], Bin Zhou[1#], Suhao Qiu[2,3#], Shengyuan Ma[2,3], Chung-Hao Lee[4], Ankush Aggarwal[5], Jianfeng Zeng[3], Mingyuan Gao[3], Yuan Feng[2,3*], Dan Li[1*], Hong Shan[1*]

[1] Guangdong Provincial Engineering Research Center of Molecular Imaging, The Fifth Affiliated Hospital, Sun Yat-sen University, Zhuhai, Guangdong, 519000, China

[2] Institute for Medical Imaging Technology, School of Biomedical Engineering, Shanghai Jiao Tong University, Shanghai, China

[3] Center for Molecular Imaging and Nuclear Medicine, School of Radiological and Interdisciplinary Sciences (RAD-X), Soochow University, Collaborative Innovation Center of Radiation Medicine of Jiangsu Higher Education Institutions, Suzhou, Jiangsu, 215123, China

[4] School of Aerospace and Mechanical Engineering, Institute for Biomedical Engineering, Science, and Technology, University of Oklahoma, Norman, OK, 73019, USA

[5] Zienkiewicz Centre for Computational Engineering, College of Engineering, Swansea University, Swansea SA1 8EN, UK


[#]Contributed equally




*Address for correspondence:
**Yuan Feng, Ph.D.**
Institute for Medical Imaging Technology
School of Biomedical Engineering
Shanghai Jiao Tong University
Shanghai, China, 200420
Email: fengyuan@sjtu.edu.cn
Tel: +86-18625085336


**Dan Li, M.D., Ph.D.**
**Hong Shan, M.D., Ph.D.**
Guangdong Provincial Engineering Research Center of Molecular Imaging
The Fifth Affiliated Hospital, Sun Yat-sen University
52 Meihuadong Rd, Zhuhai, 519000, P.R. China
Email: lidan25@mail.sysu.edu.cn
          shanhong@mail.sysu.edu.cn
Tel/Fax: +86-756-2528636

# Abstract

Photothermal therapy (PTT) has been emerging as an effective, minimally invasive approach to treat cancers. However, a method to quantitatively evaluate the treatment effect after Laser-Induced Thermotherapy (LITT) is needed. In this study, we used 808 nm laser radiation with 3 different power densities to treat the breast cancer tissue from 4T1 cell lines in a mouse model. The viscoelastic properties of the treated cancer tissues were characterized by a 2-term Prony series using a ramp-hold indentation method. We observed the instantaneous shear modulus $G_0$ was significantly higher for the treated cancer tissues than that of the untreated tissue when treated with a power density of 1.5 W/cm$^2$, but significantly lower with a power density of 2.5 W/cm$^2$. The long-term shear modulus $G_\infty$ was also significantly higher for the cancer tissue at 1.5 W/cm$^2$, compared to the untreated tissue. The treatment effects were verified by estimating the cell apoptosis rate using terminal deoxynucleotidyl transferase dUTP nick end labeling (TUNEL). Our results indicate that the viscoelastic properties of the tissue could potentially be used as biomarkers for evaluating the LITT treatment effect. In addition, we also observed a strain-independent behavior of the treated cancer tissue, which provided useful information for applying *in vivo* imaging method such as MR elastography (MRE) for treatment evaluation based on biomechanical properties.

**Keywords:** breast cancer; Laser-Induced Thermotherapy; biomechanics; viscoelastic properties; treatment evaluation.

# 1 Introduction

Cancer becomes an important leading cause of death in developing countries. Tumor resistance to various conventional treatments leads to rapid tumor growth and high possibility of tumor recurrence and metastasis. Breast cancer is the prevailing cancer with the highest number of reported cases each year, and with the highest occurrence rate for females [1]. The incidence of breast cancer in the world is increasing at 3% annually, and the age of the patient population is decreasing [2]. Clinical treatments for breast cancer include radical surgery, chemotherapy, and radiotherapy. Among these, therapies such as chemotherapy and radiotherapy have adverse side effects, especially in systemic chemotherapy [3]. Recently, photothermal therapy (PTT), a minimally invasive therapeutic approach, has emerged as a useful tool for treating cancer. PTT uses near-infrared (NIR) light-absorbing agents to convert photons into heat for inducing ablation, degeneration, and necrosis of the cancer tissues [4,5]. PTT has many advantages such as a high selectivity of the treatment target, minimal side effects, and maximal preservation of the benign tissue [6,7]. It is possible to modulate the power density with respect to the tumor size, thus enhancing the efficacy of inducing cell apoptosis [8-11]. Therefore, PTT has great potential to serve as an effective tool for treating breast cancer. However, an effective way to evaluate the Laser-Induced thermotherapy (LITT) treatment effect, quantifying the changes of the cancer tissue after treatment, is needed for accurate clinical evaluations and applications.

Common practices of assessing the therapeutic effect of breast cancer treatment include diagnostic imaging such as magnetic resonance (MR) imaging or CT scan (The Response Evaluation Criteria In Solid Tumors (RECIST) guideline) [12]. Based on the observations of the images, the tumor size, lesions changes, and metastatic regions are assessed for evaluating the treatment effect [13, 14]. However, the observations are often qualitative and largely depend on the experience of the observer. In the cellular level, estimation of the tumor cell apoptosis using

2

terminal deoxynucleotidyl transferase dUTP nick end labeling (TUNEL) are usually used [15, 16]. Although cellular level evaluations could provide more quantitative assessment, it involves complicated sectioning and staining procedures which takes days to be obtained. Therefore, an effective, quantitative, and efficient way to evaluate the treatment effects is desirable.

It is known that biomechanical properties of the cancer tissues and cells are closely related to cancer pathology and metastasis state [17-21]. For breast cancer tissues, studies have found cancer tissues to be stiffer than the normal tissues [22-24]. Additionally, in terms of viscoelastic properties, significant differences were found between the cancerous and normal tissues [20, 25, 26]. Besides *ex vivo* mechanical testing, *in vivo* imaging techniques such as MR elastography (MRE) and ultrasound elastography were also used to distinguish the breast cancer based on the biomechanical features [27-32]. However, *ex vivo* mechanical testing serves as an indispensable way for guiding the modeling and verification for in vivo measurements. Among the many *ex vivo* testing techniques, indentation proved to be an effective way for tissue characterization [33-35].

In this study, we characterized the viscoelastic properties of the breast cancer tissue after LITT. Treatment effect was evaluated by comparing the viscoelastic properties of the treated and untreated tissues for the three different power densities applied. Cellular apoptosis were evaluated by estimating the ratio of the apoptosis cells. Implications of the viscoelastic properties on the treatment effect and the cellular level responses were discussed.

## 2 Materials and Methods

### 2.1 Animal model

Eighteen (n=18) healthy female nude mice aged 4-5 weeks were used in this study. All mice were raised in the Laboratory Animal Center of Soochow University (SPF grade, certificate No.

SCXK 2002–0008). Each mouse received subcutaneous injections of 4T1 cell line (Shanghai Cell Bank of Chinese Academy of Sciences) for tumor implantation. The cells were re-suspended with phosphate-buffered saline (PBS) solutions at a concentration of $10^7$ mL$^{-1}$. A cell suspension of 50 µL was injected on both sides of the hind legs of the mice. The mice were raised for 10-14 days till palpable solid tumors with a diameter of 8-10 mm were detected (Figure **1**a).  All of the animal procedures and protocols were approved by the Institutional Animal Care and Use Committee of the Soochow University and conducted in accordance with the National Institutes of Health Guide for the Care and Use of Laboratory Animals.

## 2.2   Laser-Induced Thermotherapy (LITT)

To evaluate the treatment effect, the tumors were treated with a laser system (MDL-N-808-10W ，Changchun New Industries Optoelectronics Technology Co. Ltd.). The mice were anesthetized by intraperitoneal injection of pentobarbital (50 mg/kg) for in-vivo LITT using an 808 nm Near-infrared (NIR) laser (Figure **1**b). Statuses of the treated tumors were monitored with a real-time imaging system. The 18 mice were divided into 3 equal groups to receive irradiation with a power density of 1.5 W/cm$^2$, 2.0 W/cm$^2$, and 2.5 W/cm$^2$ for 10 minutes, respectively. For each mouse, the subcutaneous tumor on one of the implanted legs was irradiated with laser and the irradiation side was chosen randomly. The tumor on the other leg was left untreated. Statuses of the treated tumors were monitored with a real-time imaging system and the temperature change was recorded via an NIR camera.

## 2.3   Sample preparation

About 6 hours after irradiation, solid tumors from both sides of the legs were removed after the mice were euthanized by cervical dislocation (Figure **1**c).  A total of 36 solid tumor samples were harvested with a thickness of 4.64±0.76 mm. Each sample was stored in PBS solution and

transferred to the indentation tester immediately after surgical resection. The indentation tests were performed at room temperature (~20ºC).

## 2.4  Indentation test and parameter estimation

A custom-built indentation device was used to characterize the viscoelastic properties of the cancer tissue (Figure **1**d). The indentation test protocol was adopted from a previous study [36]. Briefly, indentation strains of 2%, 4%, 6%, 8%, and 10% with respect to the sample thickness were carried out with a strain rate of ~0.1 $s^{-1}$ for each sample. The force-displacement curves of the ramp-hold tests were acquired, and the data were fitted with a 2-term Prony series. Then, the reaction forces during the ramp ($0 \leq t \leq t_r$) stage and the relaxation ($t_r \leq t$) stage were [36]

$$
F = \begin{cases} 8RXV\left( C_0 t - \sum_{i=1}^{2} \tau_i C_i \left( e^{-\frac{t}{\tau_i}} - 1 \right) \right) & (0 \leq t \leq t_r) \\ 8RXV\left( C_0 t_R + \sum_{i=1}^{2} \tau_i C_i e^{-\frac{t}{\tau_i}} \left( e^{\frac{t_R}{\tau_i}} - 1 \right) \right) & (t_r \leq t) \end{cases}, \tag{1}
$$

where $R$ is the radius of the indenter, $X$ is the compensation factor for the infinite half space assumption, $V$ is the indentation velocity, $C_0$, $C_i$, and $\tau_i$ are model parameters of the 2-term Prony series for shear modulus. The corresponding instantaneous shear modulus $G_0$ and long-time shear modulus $G_\infty$ can be computed by

$$
G_0 = G(0) = C_0 + \sum_{i=1}^{2} C_i \text{ and } G_\infty = G(\infty) = C_0. \tag{2}
$$

Both the ramp and relaxation sections of the piecewise function were used for parameter estimations. The objective function with equal weights for the ramp and relaxation sections was used to estimate the viscoelastic parameters by fitting Eq. (1) to the reaction force versus time data. An in-house MATLAB (MathWorks, Natick, MA, USA) program was used to minimize the fitting error by using the "*fmincon*" function.

## 2.5 Histology and statistical analyses

Apoptosis of the cancer cells is one of the criteria to evaluate the treatment effect. Therefore, TUNEL was used for the apoptosis characterization. We first harvested the tissues in formaldehyde solution after indentation test. Then, a total of 36 treated subcutaneous cancer tissues were embedded with paraffin and sectioned. The tissue sections were stained with TUNEL apoptosis assay kit (Beyotime Institute of Biotechnology, Shanghai, China) before microscopy observation.

For a fixed field of view (FOV) in one stained slice, the ratio of the apoptosis cells $\phi_{apoptosis}$ was estimated by the fractional area of the apoptosis cells with respect to the whole area of all cells

$$\phi_{apoptosis} = \frac{A_{apoptosis}}{A - A_{gap}}, \tag{3}$$

where $A_{apoptosis}$ is the area of the apoptosis cells in the FOV, $A_{gap}$ is the gap spaces in the stain slices, and $A$ is the overall area of the FOV. The differences were compared by estimating 6 different FOVs from each mouse of the 3 power density group.

A two-way analysis of variance (ANOVA) test of the $G_\infty$ and $G_0$ values followed by a Bonferroni test (significance level of 0.05) was used to evaluate the significances of the treatment effect and the strain levels for each power density applied. The effects of power densities were compared by calculating the ratios of the $G_\infty$ and $G_0$ values for the treated and untreated tumor samples. A two-way ANOVA was also used for evaluating the influences of the power densities. The significance of $\phi_{apoptosis}$ was evaluated using a student t-test (significance level of 0.05).

# 3  Results

## 3.1  Tumor temperature during LITT treatment

The temperature distribution of the mouse body showed a concentration of high temperatures at the tumor site after LITT treatment (Figure 2a). Visible bright spots indicating the tumor locations were observed for the power densities of 2.0 W/cm$^2$ and 1.5 W/cm$^2$. Records of temperature variation over time at the tumor sites showed monotonically increasing trend for the three power densities applied (Figure 2b). The maximum temperature observed was about 62.0$^{\circ}$ C, 53.0$^{\circ}$ C and 44.0$^{\circ}$ C for the power density of 2.5 W/cm$^2$, 2.0 W/cm$^2$, and 1.5 W/cm$^2$ after 10min of irradiation, respectively.

## 3.2  Viscoelastic properties of the treated and untreated tissues

Experimental force-displacement curves from the ramp-hold test of indentation were fitted with Eq. (1) to estimate the viscoelastic parameters (Figure **3**a). Variations of the experimental data were shown by plotting the average relaxation curves and deviation regions (Figure **3**b).

The estimated viscoelastic model parameters for the tissue samples with power densities of 1.5 W/cm$^2$, 2.0 W/cm$^2$, and 2.5 W/cm$^2$ are summarized in Table **1**, Table **2**, and Table 3, respectively. Comparing the treated and untreated cancer tissues showed both $G_0$ and $G_\infty$ values were higher for the treated samples with a power density of 1.5 W/cm$^2$, at all strain levels (Figure 4).  For LITT with 2.0 W/cm$^2$, the differences between the treated and untreated tissues became smaller, with the mean $G_0$ value of the untreated tissues larger than that of treated in 2% strain. For 2.5 W/cm$^2$, the $G_0$ values kept decreasing for the treated tissues, which were smaller than that of the untreated tissues for all strain levels.  A similar trend was also observed for the $G_\infty$ values. The maximum and minimum $G_0$ values observed for the 1.5 W/cm$^2$, 2.0 W/cm$^2$, and 2.5 W/cm$^2$ were 3.32 kPa and 2.27 kPa, 2.36 kPa and 2.18 kPa, 2.16 kPa and 1.89 kPa, respectively.

For $G_\infty$, the maximum and minimum values were 0.91 kPa and 0.47 kPa, 1.20 kPa and 0.44 kPa, 1.07 kPa and 0.52 kPa, respectively.

The two-way ANOVA tests showed that, in terms of both $G_0$ and $G_\infty$ values, significant differences were found between the treated and untreated tissues for the 1.5 W/cm² group, but not for the 2.0 W/cm² group. Only the $G_0$ values were significantly different between the treated and untreated tissues for the 2.5 W/cm² group. In terms of $G_0$ values, no significant differences were found between each indentation strain levels for all the power density groups. In terms of $G_\infty$ values, the only significant differences were observed between 2% and 10% strain in the 2.0 W/cm² and 2.5 W/cm² groups, and between 2% and 8% strain in the 2.5 W/cm² group.

The influence of the applied power density was shown by the ratios of $G_0$ and $G_\infty$ values, defined as the treated moduli divided by the untreated moduli (Figure **5**). Two-way ANOVA tests showed significant differences between power densities of 2.5 W/cm² and 2.0 W/cm² for both ratios. A significant difference was also observed between 2.5 W/cm² and 1.5 W/cm² for the $G_0$ ratios.

For the relaxation of 60% of the peak indentation force, we observed the maximum relaxation time were 10.97 s, 29.13 s and 53.67 s for the 1.5 W/cm², 2.0 W/cm² and 2.5 W/cm² groups, respectively. The minimum relaxation times were 2.92 s, 3.20 s and 4.44 s, respectively (**Table 4**). Two-way ANOVA tests of the relaxation time showed no significant differences of the 60% relaxation time between the treated and untreated tissues for the 1.5 W/cm² and 2.0 W/cm² groups (Figure **6**a-b). However, significant differences of the relaxation time were found for the 2.5 W/cm² group (Figure **6**c).

## 3.3 Apoptosis ratio

TUNEL stain showed that there are great differences when tumors suffered from different irradiation power densities (Figure **7**). Under 400x microscopy, we can find the apoptosis ratio of each sample from treated and untreated groups. The estimated $\phi_{apoptosis}$ values were

10%$\pm$12.39%, 19%$\pm$7.83%, and 21%$\pm$8.45% for the power densities of 1.5 W/cm$^2$, 2.0 W/cm$^2$, and 2.5 W/cm$^2$ (**Table 5**). For the untreated group, the estimated $\phi_{apoptosis}$ values were 8%$\pm$9.13%, 4%$\pm$ 5.00%, and 5%$\pm$7.28% respectively.

## 4   Discussion

In this study, we characterized the mechanical properties of breast cancer tissue from 4T1 cell lines after LITT with a mouse model. Using an indentation method, we observed viscoelastic properties could be used to distinguish the treated and untreated cancer tissues, and the differences between the power density of 1.5W/cm$^2$, 2.0W/cm$^2$ and 2.5W/cm$^2$. Comparisons of the measured viscoelastic moduli at different strain levels showed largely linear behavior. Analysis of the apoptosis ratio of different power density showed to be closely related to the mechanical properties of the tissue.

### 4.1   Viscoelastic properties of the treated cancer tissues

Studies have already shown that mechanical properties could be used to distinguish normal and cancer tissues [23, 28, 37-39]. Most of the studies investigated the elastic properties of the human breast cancer tissue.  Although clinically relevant, it is hard to carry out systematic treatment evaluations. In this animal-based study, we characterized and compared the viscoelastic properties of the breast cancer tissue after laser treatment.  Although LITT has emerged as an effective tool, limited studies have been carried out with respect to its treatment evaluation. We found that after thermotherapy, the elastic properties of the tissues were within the range of the previous results.

For $G_0$ and $G_\infty$ values, no significant differences were observed across the strain levels of 4%-10%. The only 3 cases that had significant differences were related with 2% indentation. This showed that the LITT treated breast cancer tissue had strain-independent properties for the short-term and long-term responses. This is similar to that of the tissues without LITT. These strain-

independent properties indicate that the breast cancer tissue after LITT treatment could be modeled and measured for *in vivo* measurements such as MR elastography [28, 40]. In fact, our results provide the first *ex vivo* measurements to support the linear viscoelastic assumptions of the breast cancer tissue after LITT.

Pre-applied stress or strain could affect the measured properties of the breast cancer tissue [21, 24]. This nonlinear behavior of the breast cancer tissue is similar to many other biological tissues in the large strain regime [35, 41]. In this study, we did not observe an apparent increase of the $G_0$ and $G_\infty$ values for the treated tissues as the strain level increased. This showed that the treated tissues did not have a larger nonlinear behavior as the untreated tissues. The variations of the relaxation time of the treated tissues also indicate that the time-domain nonlinear effect is also needed for viscoelastic modeling of the cancer tissue.

## 4.2 Treatment evaluations

Commonly used treatment evaluation methods for the treatment of breast cancer such as measurement of tumour size, checking metastasis state could only provide qualitative estimate. We showed that biomechanical properties of the treated breast cancer tissue are closely related to the power density applied and the cancer cell apoptosis. These results could be used for imaging methods such as MRE for *in vivo* treatment evaluation. In fact, elastography method using ultrasound has been used to assess the relative change of the tumor stiffness to predict the early treatment response to chemotherapy [42]. In addition, unlike the *ex vivo* testing methods such as TUNEL stain that takes days of work to be fixed, stained, and observed, biomechanical characterization methods provide a potentially more efficient and convenient alternative.

As the power density value increased, the $G_0$ value of the treated tumor tissue decreased compared to the untreated tissue. The treated tumor tissues were significantly stiffer than the normal tissues with 1.5W/cm$^2$ laser irradiation, but became significantly softer with 2.5W/cm$^2$. The transition 2.0W/cm$^2$ showed no significant differences between the treated and untreated tissues.

This tissue level biomechanical feature is consistent with the TUNEL observation with the cell apoptosis increased with the power densities applied. Since the tumor tissue is stiffer than the normal tissue in its natural state, these results indicate that LITT with 1.5W/cm$^2$ did not introduce much treatment effect while the LITT with 2.5W/cm$^2$ induced large enough apoptosis for the tissue level changes. Studies have shown that extra cellular matrix (ECM) plays a key role in determining the tissue stiffness [43]. Therefore, we postulate that the application of LITT not only induced the apoptosis of the cancer cells, but also destroyed the ECM structures of the tissue.

Significant differences in the long-term shear modulus $G_\infty$ were only observed at the 1.5W/cm$^2$. However, only the tissues after LITT with 2.5W/cm$^2$ showed to have significant different 60% relaxation time. This indicates that the apoptosis of the cancer cells did not contribute to the long-term elastic behavior as much as the short-term behavior. The larger relaxation time, especially for the 2.5W/cm$^2$ group, also showed that the tissue tends to take a longer time to recover, which is another indication of the ECM damage by LITT.

## 4.3 Limitations and future studies

Factors, such as tumor growth, sample moisture and tissue homogeneity, could contribute to the experimental errors. For the untreated tumor tissues, tissue was not checked for necrosis, which may influence the tissue properties. In addition, TUNEL stain may suffer from FOV selections deviated from the actual treated region or selection of necrosis areas. Future studies include investigation of the ECM in the breast cancer tissue after treatment, and mechanotransduction studies of the cancer tissues.

# 5  Conclusions

Viscoelastic properties of the breast cancer tissue treated by LITT were measured using a custom-built indentation device. Comparisons between the short-term shear moduli $G_0$ based on a 2-term Prony series showed they had significant values in distinguishing treated and untreated

tumor tissues for the power densities of 1.5 W/cm$^2$ and 2.5 W/cm$^2$. The ratios of $G_0$ between the treated and untreated tumor tissues also showed significant differences between the 2.5 W/cm$^2$ group and the other two power density groups. The long-term shear moduli $G_\infty$ also showed significant differences to distinguish the treated and untreated tumor tissues for the 1.5 W/cm$^2$ group, and the corresponding ratios to distinguish the treatment of 2.5 W/cm$^2$ vs. 2.0 W/cm$^2$. Analysis with estimates of cell apoptosis indicated that the degenerations of the tumor cells could contribute to the short-term biomechanical responses of the cancer tissue. In addition, for both shear moduli, strain-independent behaviors were observed for the treated cancer tissues. This indicates that in vivo imaging methods such as MRE could also be used to measure the treated breast cancer tissues. These results provide insights into the biomechanical responses of the breast cancer tissue after LITT, which is helpful for modeling the treatment procedure in the tissue level. Results also indicate that the viscoelastic properties could potentially serve as biomarkers for treatment evaluation. The measured parameters could also help validating and improving image-based elastography method such MRE for treatment evaluation.

# 6  Conflict of interest statement

No conflict of interest exists.

# 7  Acknowledgement

# 8 References

[1] Siegel, R. L., Miller, K. D., and Jemal, A., 2016, "Cancer statistics, 2016," CA: A Cancer Journal for Clinicians, 66(1), pp. 7-30.

[2] Lu, W. L., Li, H. X., Qian, B. Y., Wang, Y., Jansen, L., Huang, G. W., Tang, N. J., Sun, Z., Chen, K. X., and De Bock, G. H., 2010, "The clinical characteristics and prognosis of Chinese early stage breast cancer patients: a retrospective study," The breast journal, 16(3), pp. 331-333.

[3] Brewster, A. M., Chavez-MacGregor, M., and Brown, P., 2014, "Epidemiology, biology, and treatment of triple-negative breast cancer in women of African ancestry," The Lancet Oncology, 15(13), pp. e625-e634.

[4] Sun, C., Wen, L., Zeng, J., Wang, Y., Sun, Q., Deng, L., Zhao, C., and Li, Z., 2016, "One-pot solventless preparation of PEGylated black phosphorus nanoparticles for photoacoustic imaging and photothermal therapy of cancer," Biomaterials, 91, pp. 81-89.

[5] Kennedy, L. C., Bickford, L. R., Lewinski, N. A., Coughlin, A. J., Hu, Y., Day, E. S., West, J. L., and Drezek, R. A., 2011, "A new era for cancer treatment: gold-nanoparticle-mediated thermal therapies," Small, 7(2), pp. 169-183.

[6] Mou, J., Li, P., Liu, C., Xu, H., Song, L., Wang, J., Zhang, K., Chen, Y., Shi, J., and Chen, H., 2015, "Ultrasmall Cu2-x S Nanodots for Highly Efficient Photoacoustic Imaging-Guided Photothermal Therapy," Small, 11(19), pp. 2275-2283.

[7] Liang, C., Diao, S., Wang, C., Gong, H., Liu, T., Hong, G., Shi, X., Dai, H., and Liu, Z., 2014, "Tumor metastasis inhibition by imaging-guided photothermal therapy with single-walled carbon nanotubes," Advanced materials, 26(32), pp. 5646-5652.

[8] Zeng, J., Cheng, M., Wang, Y., Wen, L., Chen, L., Li, Z., Wu, Y., Gao, M., and Chai, Z., 2016, "pH-Responsive Fe(III)-Gallic Acid Nanoparticles for In Vivo Photoacoustic-Imaging-Guided Photothermal Therapy," Advanced healthcare materials, 5(7), pp. 772-780.

[9] Su, X., Fu, B., and Yuan, J., 2017, "Gold nanocluster-coated gold nanorods for simultaneously enhanced photothermal performance and stability," Materials Letters, 188, pp. 111-114.

[10] Yong Y, Cheng X, Bao T, and Y, Z., 2015, "Tungsten sulfide quantum dots as multifunctional nanotheranostics for In Vivo dual-modal image-guided photothermal/radiotherapy synergistic therapy," ACS nano, 9(12), pp. 12451-12463.

[11] Li, Z., Wang, H., Chen, Y., Wang, Y., Li, H., Han, H., Chen, T., Jin, Q., and Ji, J., 2016, "pH- and NIR Light-Responsive Polymeric Prodrug Micelles for Hyperthermia-Assisted Site-Specific Chemotherapy to Reverse Drug Resistance in Cancer Treatment," Small, 12(20), pp. 2731-2740.

[12] Eisenhauer, E. A., Therasse, P., Bogaerts, J., Schwartz, L. H., Sargent, D., Ford, R., Dancey, J., Arbuck, S., Gwyther, S., Mooney, M., Rubinstein, L., Shankar, L., Dodd, L., Kaplan, R., Lacombe, D., and Verweij, J., 2009, "New response evaluation criteria in solid tumours: revised RECIST guideline (version 1.1)," European journal of cancer (Oxford, England : 1990), 45(2), pp. 228-247.

[13] Li, X., Ferrel, G. L., Guerra, M. C., Hode, T., Lunn, J. A., Adalsteinsson, O., Nordquist, R. E., Liu, H., and Chen, W. R., 2011, "Preliminary safety and efficacy results of laser immunotherapy for the treatment of metastatic breast cancer patients," Photochem Photobiol Sci, 10(5), pp. 817-821.

[14] Tokes, T., Kajary, K., Szentmartoni, G., Lengyel, Z., Gyorke, T., Torgyik, L., Somlai, K., Tokes, A. M., Kulka, J., and Dank, M., 2017, "Predictive and prognostic value of FDG-PET/CT imaging and different response evaluation criteria after primary systemic therapy of breast cancer," Breast cancer, 24(1), pp. 137-146.

[15] Ana Carolina B.M. Martin, Angelina M. Fuzer, and B, A., 2017, "[10]-gingerol induces apoptosis and inhibits metastatic dissemination of triple negative breast cancer in vivo," Oncotarget, 8(42), pp. 72260-72271.

[16] Christina SHINTIA, Hardjolukito ENDANG, and DIANI, K., 2016, "Assessment of pathological response to neoadjuvant chemotherapy in locally advanced breast cancer using the Miller-Payne system and TUNEL," Malaysian J Pathol, 38(1), pp. 25-32.

[17] Suresh, S., Spatz, J., Mills, J. P., Micoulet, A., Dao, M., Lim, C. T., Beil, M., and Seufferlein, T., 2005, "Connections between single-cell biomechanics and human disease states: gastrointestinal cancer and malaria," Acta Biomaterialia, 1(1), pp. 15-30.

[18] Suresh, S., 2007, "Biomechanics and biophysics of cancer cells," Acta Biomaterialia, 3(4), pp. 413-438.

[19] Genin, G. M., Shenoy, V. B., Peng, G. C. Y., and Buehler, M. J., 2017, "Integrated Multiscale Biomaterials Experiment and Modeling," ACS Biomaterials Science & Engineering, 3(11), pp. 2628-2632.

[20] Madani, N., and Mojra, A., 2017, "Quantitative diagnosis of breast tumors by characterization of viscoelastic behavior of healthy breast tissue," J Mech Behav Biomed, 68, pp. 180-187.

[21] Ramião, N. G., Martins, P. S., Rynkevic, R., Fernandes, A. A., Barroso, M., and Santos, D. C., 2016, "Biomechanical properties of breast tissue, a state-of-the-art review," Biomech Model Mechanobiol, 15(5), pp. 1307-1323.

[22] Samani, A., Bishop, J., Luginbuhl, C., and Plewes, D. B., 2003, "Measuring the elastic modulus of ex vivo small tissue samples," Physics in Medicine and Biology, 48(14), p. 2183.

[23] Samani, A., Zubovits, J., and Plewes, D., 2007, "Elastic moduli of normal and pathological human breast tissues: an inversion-technique-based investigation of 169 samples," Physics in medicine and biology, 52(6), p. 1565.

[24] Krouskop, T. A., Wheeler, T. M., Kallel, F., Garra, B. S., and Hall, T., 1998, "Elastic moduli of breast and prostate tissues under compression," Ultrasonic imaging, 20(4), pp. 260-274.

[25] Mojra, A., Najarian, S., Kashani, S. M. T., and Panahi, F., 2012, "A novel tactile-guided detection and three-dimensional localization of clinically significant breast masses," Journal of Medical Engineering & Technology, 36(1), pp. 8-16.

[26] Mojra, A., Najarian, S., Towliat Kashani, S. M., Panahi, F., and Yaghmaei, M., 2011, "A novel haptic robotic viscogram for characterizing the viscoelastic behaviour of breast tissue in clinical examinations," The international journal of medical robotics + computer assisted surgery : MRCAS, 7(3), pp. 282-292.

[27] Mariappan, Y. K., Glaser, K. J., Manduca, A., Romano, A. J., Venkatesh, S. K., Yin, M., and Ehman, R. L., 2009, "High-Frequency Mode Conversion Technique for Stiff Lesion Detection with Magnetic Resonance Elastography (MRE)," Magn Reson Med, 62(6), pp. 1457-1465.

[28] Sinkus, R., Tanter, M., Xydeas, T., Catheline, S., Bercoff, J., and Fink, M., 2005, "Viscoelastic shear properties of in vivo breast lesions measured by MR elastography," Magnetic Resonance Imaging, 23(2), pp. 159-165.

[29] Chang, J. M., Won, J.-K., Lee, K.-B., Park, I. A., Yi, A., and Moon, W. K., 2013, "Comparison of Shear-Wave and Strain Ultrasound Elastography in the Differentiation of Benign and Malignant Breast Lesions," American Journal of Roentgenology, 201(2), pp. W347-W356.

[30] Coussot, C., Kalyanam, S., Yapp, R., and Insana, M. F., 2009, "Fractional derivative models for ultrasonic characterization of polymer and breast tissue viscoelasticity," IEEE Trans Ultrason Ferroelectr Freq Control, 56(4), pp. 715-726.

[31] Ophir, J., Garra, B., Kallel, F., Konofagou, E., Krouskop, T., Righetti, R., and Varghese, T., 2000, "Elastographic imaging," Ultrasound Med Biol, 26 Suppl 1, pp. S23-29.

[32] Han, Y., Wang, S., Hibshoosh, H., Taback, B., and Konofagou, E., 2016, "Tumor characterization and treatment monitoring of postsurgical human breast specimens using harmonic motion imaging (HMI)," Breast Cancer Res, 18(1), p. 46.

[33] Feng, Y., Lee, C.-H., Sun, L., Ji, S., and Zhao, X., 2017, "Characterizing white matter tissue in large strain via asymmetric indentation and inverse finite element modeling," J Mech Behav Biomed, 65, pp. 490-501.

[34] Feng, Y., Gao, Y., Wang, T., Tao, L., Qiu, S., and Zhao, X., 2017, "A longitudinal study of the mechanical properties of injured brain tissue in a mouse model," J Mech Behav Biomed, 71, pp. 407-415.

[35] Feng, Y., Okamoto, R. J., Namani, R., Genin, G. M., and Bayly, P. V., 2013, "Measurements of mechanical anisotropy in brain tissue and implications for transversely isotropic material models of white matter," J Mech Behav Biomed, 23, pp. 117-132.

[36] Qiu, S., Zhao, X., Chen, J., Zeng, J., Chen, S., Chen, L., Meng, Y., Liu, B., Shan, H., Gao, M., and Feng, Y., 2018, "Characterizing viscoelastic properties of breast cancer tissue from 4T1 and SKBR3 cell lines with indentation using a mouse model," J Biomech, 69, pp. 81-89.

[37] Joseph, J. O. H., and Samani, A., 2009, "Measurement of the hyperelastic properties of 44 pathological ex vivo breast tissue samples," Physics in Medicine and Biology, 54(8), p. 2557.

[38] Plodinec, M., Loparic, M., Monnier, C. A., Obermann, E. C., Zanetti-Dallenbach, R., Oertle, P., Hyotyla, J. T., Aebi, U., Bentires-Alj, M., and Lim, R. Y., 2012, "The nanomechanical signature of breast cancer," Nature nanotechnology, 7(11), pp. 757-765.

[39] Umemoto, T., Ueno, E., Matsumura, T., Yamakawa, M., Bando, H., Mitake, T., and Shiina, T., 2014, "Ex vivo and in vivo assessment of the non-linearity of elasticity properties of breast tissues for quantitative strain elastography," Ultrasound Med Biol, 40(8), pp. 1755-1768.

[40] Griesenauer, R. H., Weis, J. A., Arlinghaus, L. R., Meszoely, I. M., and Miga, M. I., 2017, "Breast tissue stiffness estimation for surgical guidance using gravity-induced excitation," Physics in Medicine and Biology, 62(12), pp. 4756-4776.

[41] Feng, Y., Okamoto, R. J., Genin, G. M., and Bayly, P. V., 2016, "On the accuracy and fitting of transversely isotropic material models," J Mech Behav Biomed, 61, pp. 554-566.

[42] Jing, H., Cheng, W., Li, Z. Y., Ying, L., Wang, Q. C., Wu, T., and Tian, J. W., 2016, "Early Evaluation of Relative Changes in Tumor Stiffness by Shear Wave Elastography Predicts the Response to Neoadjuvant Chemotherapy in Patients With Breast Cancer," Journal of ultrasound in medicine : official journal of the American Institute of Ultrasound in Medicine, 35(8), pp. 1619-1627.

[43] Collins, C., Osborne, L. D., Guilluy, C., Chen, Z., O'Brien, E. T., 3rd, Reader, J. S., Burridge, K., Superfine, R., and Tzima, E., 2014, "Haemodynamic and extracellular matrix cues regulate the mechanical phenotype and stiffness of aortic endothelial cells," Nat Commun, 5, p. 3984.

Figure 1. Mouse and schematic diagram of irradiation and indentation test.

Figure 2. Temperature curve and Laser photothermal imaging.

Figure 3. Typical experimental and fitted curves.

Figure 4. Comparisons of the treated and untreated tissues in terms of power density.

Figure 5. Comparisons of ratio from dividing the modulus of the treated tissue with that of the untreated tissue.

Figure 6. TUNEL staining and apoptosis calculation.

Figure 7. Comparisions of relaxation time of the treated and untreated tumor tissues.
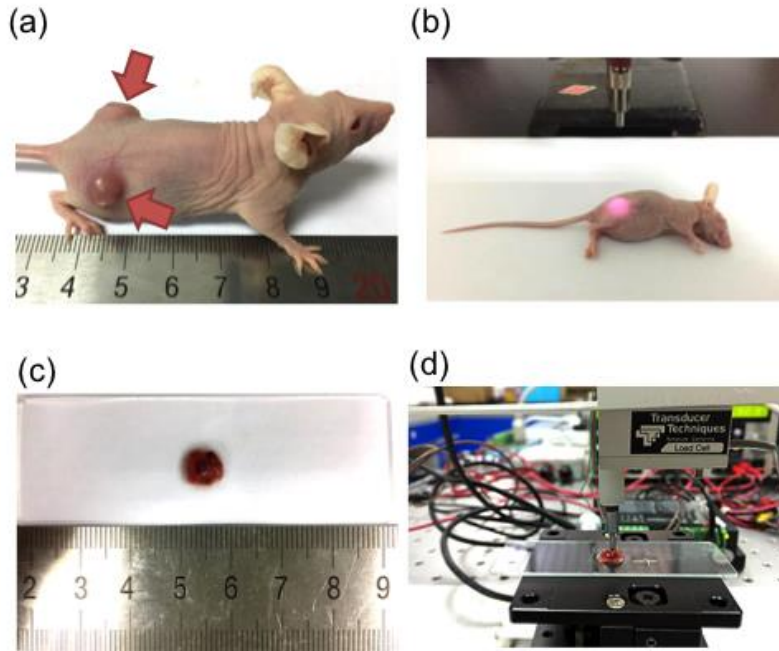
Figure 1.(a) Two solid tumors (red arrows) implanted on both sides of the rear leg of a mouse after injection of 4T1 cancer cells subcutaneously. (b) Irradiation of the implanted tumor with an 808 nm laser. (c) A tissue sample of solid tumor dissected for measurements. (d) Indentation of a tissue sample with a cylindrically shaped indenter.
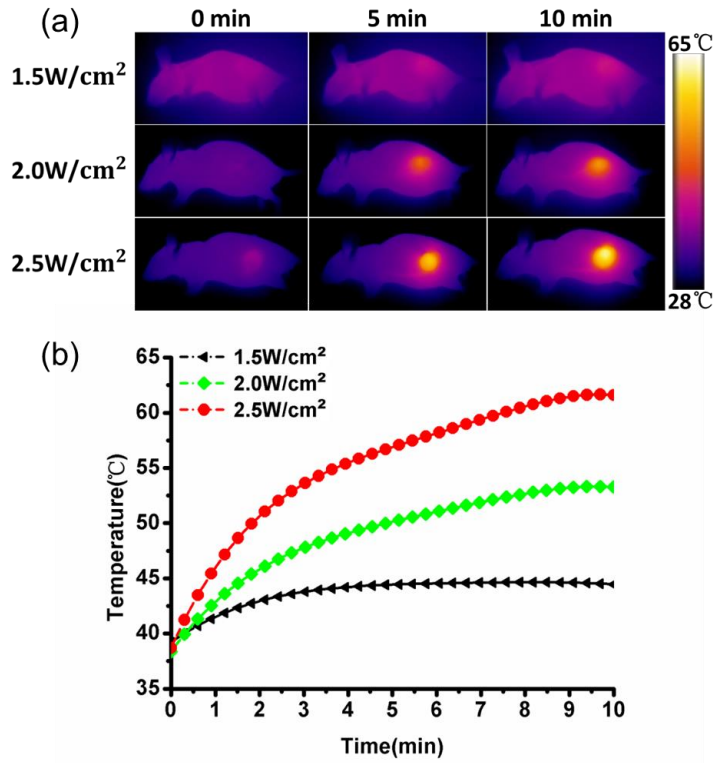
Figure 2. (a) Distributions of the mouse body temperature during photothermal imaging. The highest temperature was observed at the tumor site after 10 min of LITT with a power density of 2.5 W/cm². (b) The temperature of the treated tumor over time under power densities of 1.5 W/cm², 2.0 W/cm², and 2.5 W/cm².
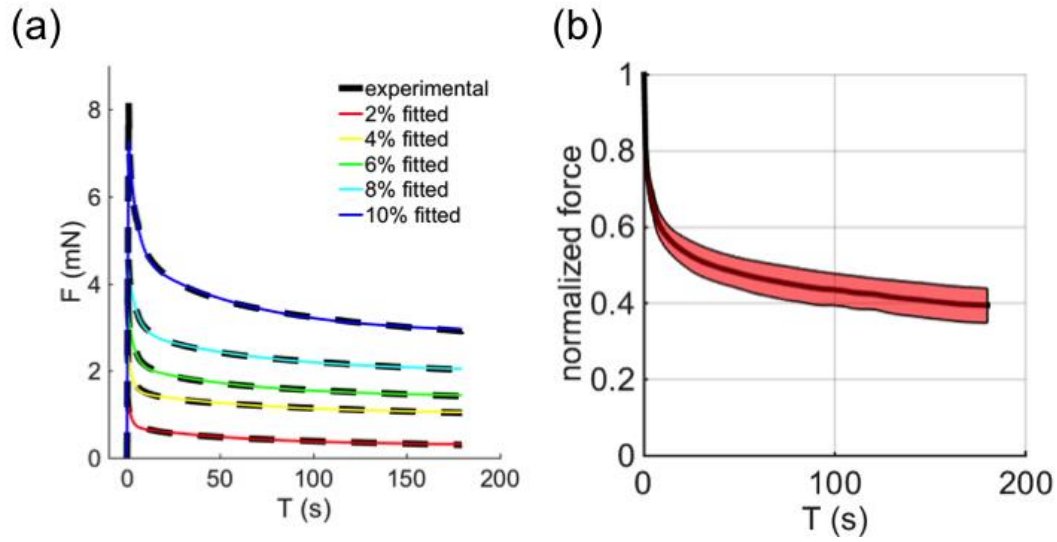
Figure 3. (a) Typical experimental and fitted force-displacement curves for indentation strain levels of 2%, 4%, 6%, 8%, and 10%. The $R^2$ values of the fittings were 0.99 for all cases. (b) A typical average force relaxation curve of 6 tumor samples with an indentation strain level of 6% (1.5W/cm$^2$). The shaded area indicates the standard deviation of the measured relaxation curves .
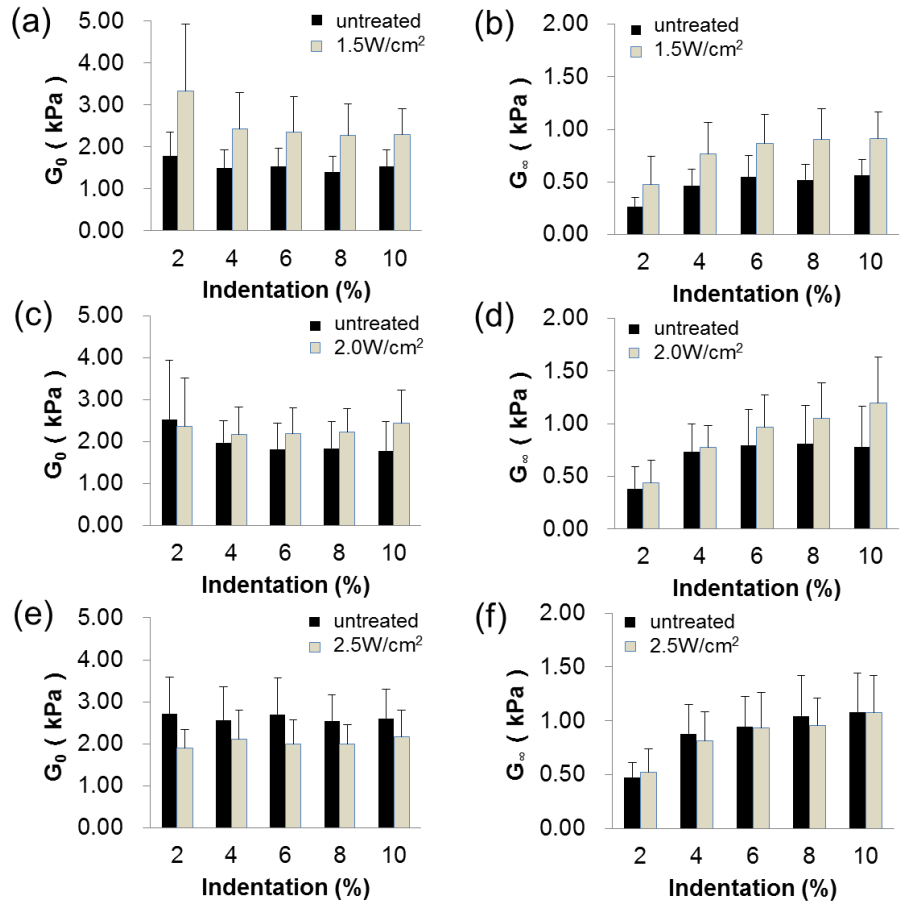
Figure 4.Comparisons of the treated and untreated cancer tissues in terms of (a, c, e) instantaneous shear modulus $G_0$, and (b, d, f) long-term shear modulus $G_\infty$ (mean$\pm$95% confidence interval). The power density applied were (a, b) 1.5 W/cm$^2$, (c, d) 2.0 W/cm$^2$, and (e, f) 2.5 W/cm$^2$.
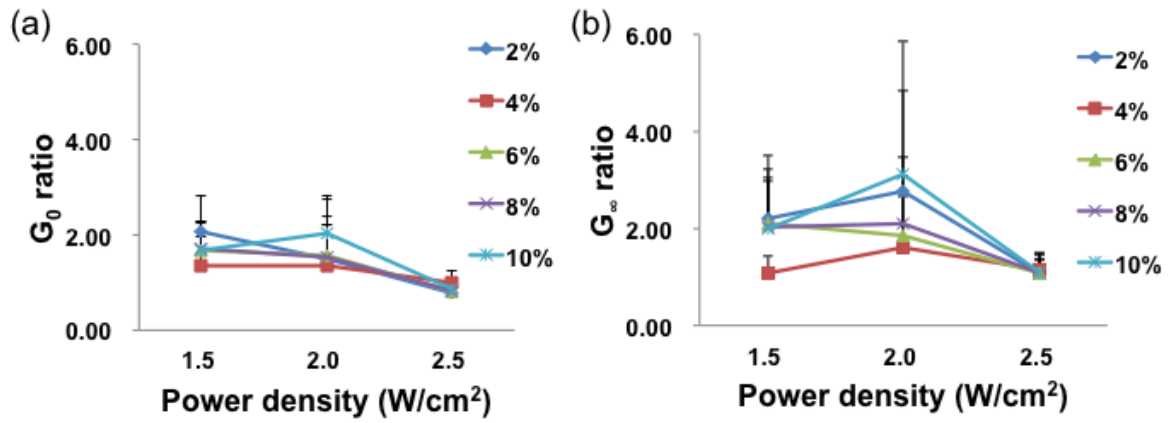
Figure 5. Ratios of (a) $G_0$ and (b) $G_\infty$ values at each indentation strain level for the three irradiation power densities (mean$\pm$95% confidence interval). The ratio was defined by dividing the modulus of the treated tissue with that of the untreated tissue.
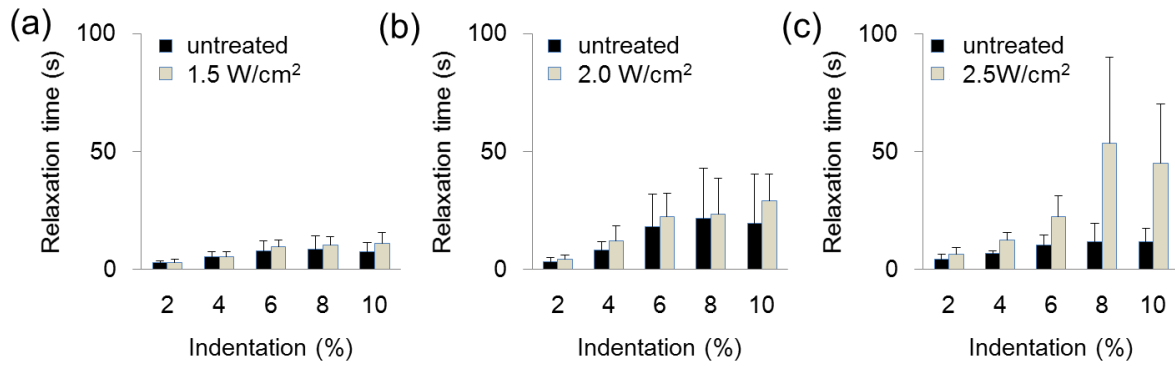
Figure 6. Relaxation time of the treated and untreated tumor tissues for the power density groups of (a) 1.5 W/cm$^2$, (b) 2.0 W/cm$^2$, and (c) 2.5 W/cm$^2$. The relaxation time was estimated based on the 60% relaxation of the average indentation force.
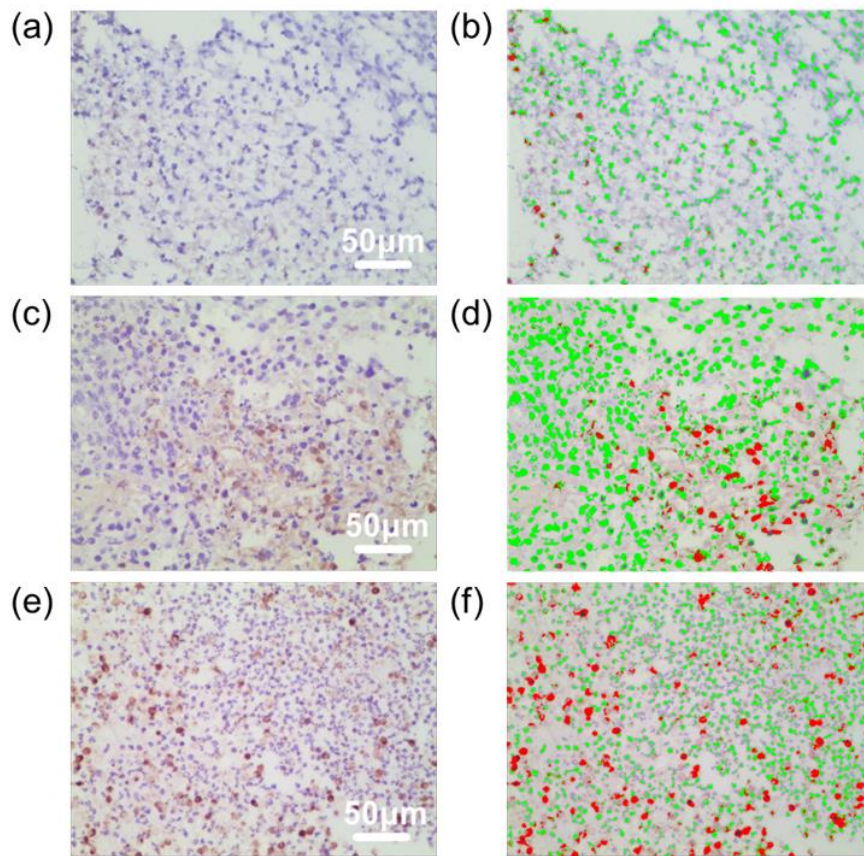
Figure 7. TUNEL stain using 400x microscopy for (a, c, e) the treated tumor tissues and (b, d, f) the corresponding labeled live and apoptosis cells. The normal tumor cells were labeled with green color and the apoptosis cells were labeled with red color. Power densities of (a, b) 1.5 W/cm$^2$, (c, d) 2.0 W/cm$^2$, and (e, f) 2.5 W/cm$^2$ are illustrated.

Table 1. Viscoelastic properties of the breast cancer tissue from 1.5W/cm2 untreated and treated groups with 95% confidence intervals.

| | Indentation strain | $G_\infty$ (kPa) | $C_1$ (kPa) | $C_2$ (kPa) | $\tau_1$ (s) | $\tau_2$ (s) | $G_0$ (kPa) | $R^2$ |
|---|---|---|---|---|---|---|---|---|
| Untreated | 2% | 0.26±0.09 | 0.93±0.31 | 0.59±0.20 | 1.72±0.44 | 55.98±12.30 | 1.78±0.58 | 0.98 |
| | 4% | 0.46±0.16 | 0.69±0.19 | 0.34±0.12 | 1.87±0.54 | 54.12±8.54 | 1.49±0.45 | 0.98 |
| | 6% | 0.55±0.20 | 0.66±0.17 | 0.32±0.11 | 2.16±0.47 | 49.63±9.73 | 1.53±0.43 | 0.98 |
| | 8% | 0.52±0.15 | 0.61±0.18 | 0.28±0.08 | 2.89±0.77 | 69.91±27.34 | 1.41±0.36 | 0.98 |
| | 10% | 0.56±0.15 | 0.55±0.17 | 0.42±0.19 | 9.77±12.06 | 43.00±16.65 | 1.53±0.40 | 0.98 |
| Treated | 2% | 0.47±0.27 | 1.90±0.94 | 0.95±0.44 | 1.18±0.76 | 59.03±16.10 | 3.32±1.60 | 0.97 |
| | 4% | 0.77±0.30 | 1.04±0.50 | 0.62±0.18 | 11.29±16.20 | 56.77±22.32 | 2.42±0.87 | 0.98 |
| | 6% | 0.87±0.27 | 0.98±0.43 | 0.50±0.20 | 2.46±0.57 | 59.70±7.33 | 2.35±0.85 | 0.99 |
| | 8% | 0.90±0.29 | 0.90±0.27 | 0.48±0.20 | 2.88±0.48 | 59.75±2.76 | 2.27±0.75 | 0.99 |
| | 10% | 0.91±0.26 | 0.86±0.34 | 0.53±0.19 | 11.70±16.04 | 50.61±19.34 | 2.29±0.61 | 0.98 |

Table 2. Viscoelastic properties of the breast cancer tissue from 2.0W/cm$^2$ untreated and treated groups with 95% confidence intervals.

| | Indentation strain | $G_\infty$ (kPa) | $C_1$ (kPa) | $C_2$ (kPa) | $\tau_1$ (s) | $\tau_2$ (s) | $G_0$ (kPa) | $R^2$ |
|---|---|---|---|---|---|---|---|---|
| Untreated | 2% | 0.38±0.21 | 1.60±1.29 | 0.55±0.11 | 1.54±0.67 | 64.54±13.43 | 2.53±1.40 | 0.98 |
| | 4% | 0.73±0.26 | 0.84±0.17 | 0.40±0.12 | 1.96±0.19 | 52.67±2.85 | 1.97±0.53 | 0.98 |
| | 6% | 0.79±0.34 | 0.66±0.19 | 0.36±0.11 | 2.78±0.30 | 58.22±4.69 | 1.82±0.62 | 0.99 |
| | 8% | 0.81±0.37 | 0.63±0.22 | 0.40±0.14 | 13.36±18.65 | 52.27±18.56 | 1.84±0.63 | 0.98 |
| | 10% | 0.78±0.39 | 0.59±0.24 | 0.40±0.16 | 12.85±16.72 | 55.95±19.90 | 1.78±0.70 | 0.99 |
| Treated | 2% | 0.44±0.21 | 1.23±0.72 | 0.70±0.25 | 10.49±16.58 | 55.78±24.78 | 2.36±1.15 | 0.98 |
| | 4% | 0.78±0.21 | 0.90±0.35 | 0.50±0.13 | 2.23±0.76 | 60.51±9.67 | 2.18±0.65 | 0.99 |
| | 6% | 0.97±0.31 | 0.69±0.19 | 0.52±0.21 | 12.23±16.85 | 53.54±18.85 | 2.18±0.61 | 0.99 |
| | 8% | 1.05±0.34 | 0.76±0.13 | 0.42±0.11 | 3.06±0.62 | 67.08±2.23 | 2.22±0.55 | 0.99 |
| | 10% | 1.20±0.44 | 0.71±0.21 | 0.54±0.19 | 14.51±19.37 | 56.53±19.74 | 2.44±0.77 | 0.99 |

Table 3. Viscoelastic properties of the breast cancer tissue from 2.5W/cm$^2$ untreated and treated groups with 95% confidence intervals.

| | Indentation strain | $G_\infty$ (kPa) | $C_1$ (kPa) | $C_2$ (kPa) | $\tau_1$ (s) | $\tau_2$ (s) | $G_0$ (kPa) | $R^2$ |
|---|---|---|---|---|---|---|---|---|
| Untreated | 2% | 0.48±0.13 | 1.47±0.72 | 0.76±0.16 | 2.29±1.03 | 65.59±11.24 | 2.71±0.87 | 0.99 |
| | 4% | 0.88±0.27 | 1.09±0.35 | 0.59±0.19 | 2.26±0.43 | 58.93±5.01 | 2.56±0.80 | 0.99 |
| | 6% | 0.94±0.28 | 1.20±0.48 | 0.55±0.16 | 2.01±0.82 | 52.91±6.74 | 2.69±0.88 | 0.98 |
| | 8% | 1.05±0.38 | 0.98±0.13 | 0.51±0.14 | 2.94±0.76 | 63.32±2.72 | 2.54±0.62 | 0.98 |
| | 10% | 1.08±0.36 | 0.88±0.25 | 0.64±0.17 | 14.22±19.53 | 51.06±17.68 | 2.60±0.70 | 0.99 |
| Treated | 2% | 0.52±0.22 | 0.84±0.11 | 0.53±0.14 | 1.67±0.65 | 58.92±10.88 | 1.89±0.44 | 0.98 |
| | 4% | 0.81±0.27 | 0.88±0.33 | 0.41±0.11 | 1.88±0.32 | 60.51±10.22 | 2.10±0.70 | 0.98 |
| | 6% | 0.93±0.33 | 0.69±0.14 | 0.37±0.12 | 2.60±0.51 | 64.66±7.19 | 1.99±0.57 | 0.99 |
| | 8% | 0.96±0.25 | 0.66±0.13 | 0.37±0.13 | 2.64±0.77 | 64.69±9.51 | 1.99±0.46 | 0.99 |
| | 10% | 1.07±0.35 | 0.63±0.19 | 0.45±0.16 | 11.71±15.31 | 61.10±21.08 | 2.16±0.64 | 0.99 |

Table 4. Relaxation time for 60% of the peak indentation force.

| | Indentation strain | 1.5W/cm$^2$ | 2.0W/cm$^2$ | 2.5W/cm$^2$ |
|---|---|---|---|---|
| Untreated | 2% | 3.02±0.50 | 3.20±1.90 | 4.44±1.98 |
| | 4% | 5.47±2.08 | 8.25±3.68 | 6.96±1.05 |
| | 6% | 7.98±4.30 | 18.28±13.80 | 10.55±3.99 |
| | 8% | 8.65±5.50 | 21.61±21.34 | 11.88±7.71 |
| | 10% | 7.48±3.93 | 19.50±20.83 | 11.95±5.67 |
| Treated | 2% | 2.92±1.51 | 4.41±1.86 | 6.41±2.84 |
| | 4% | 5.29±2.45 | 12.19±6.25 | 12.38±3.50 |
| | 6% | 9.84±2.80 | 22.43±9.81 | 22.50±8.77 |
| | 8% | 10.44±3.34 | 23.54±15.04 | 53.67±36.29 |
| | 10% | 10.97±4.71 | 29.13±11.17 | 45.17±25.18 |

Table 5. Cell apoptosis ratio for each sample with the irradiation power density of 1.5 W/cm$^2$, 2.0 W/cm$^2$, and 2.5 W/cm$^2$.

|  | 1.5 W/cm$^2$ | 2.0 W/cm$^2$ | 2.5 W/cm$^2$ |
|---|---|---|---|
| | 3% | 26% | 16% |
| | 0% | 30% | 25% |
| | 20% | 11% | 27% |
| Treated | 5% | 19% | 23% |
| | 30% | 16% | 7% |
| | 0% | 11% | 30% |
| | 10% | 6% | 2% |
| | 0% | 0% | 0% |
| | 0% | 0% | 0% |
| Untreated | 18% | 0% | 6% |
| | 0% | 12% | 2% |
| | 19% | 7% | 19% |